Electronic Supplementary Information

A Bis(triisopropylsilylethynyl)-Substituted Pyrene-Fused Tetraazaheptacene: Synthesis and Properties

Contents page

1. General experimental methods

Compounds **2**,[1] **3**[2] and **4**[3] were prepared according to reported procedures.

Reagents for synthesis were, if not otherwise specified, purchased from Aldrich, Fluka or Acros. Commercial chemicals and solvents were used as received. Anhydrous THF was dried using an Innovative Pure Solve solvent purification system.

Column chromatography was carried out using Silica gel 60 (40-60 μm) from Scharlab. Analytical thin layer chromatography (TLC) was done using aluminum sheets (20x20 cm) pre-coated with silica gel RP-18W 60 F254 from Merck. UV-active compounds were detected with a UV-lamp from CAMAG at wavelength λ = 254 or 366 nm.

Absorption an emission spectra were recorded on a Perkin-Elmer *Lambda 950* spectrometer, and a *LS55* Perkin-Elmer Fluorescence spectrometer, respectively. Anhydrous 1,2-dichlorobenzene from Sigma-Aldrich was used as purchased.

Electrochemical measurements were carried out on a Princeton Applied Research Parstat 2273 in a 3-electrode single compartment cell with Pt disc working electrode (Ø = 0.5 mm), a platinum wire counter electrode (Ø = 0.5 mm) and a silver wire pseudoreference electrode. The cell and the electrodes were custom made. The reduction potentials were referred to SCE using ferrocene (Fc) as internal reference ($E_{1/2}$ Fc (SCE) = +0.48 V) after the measurements.

NMR spectra were recorded on Bruker Avance 400 spectrometer at 298 K using partially deuterated solvents as internal standards. Coupling constants (*J*) are denoted in Hz and chemical shifts (δ) in ppm. Multiplicities are denoted as follows: s = singlet, d = doublet, t = triplet, m = multiplet, br = broad.

Matrix Assisted Laser Desorption Ionization (coupled to a Time-Of-Flight analyzer) experiments (MALDI-TOF) were recorded on Bruker REFLEX spectrometer in Polymat by Dr. Antonio Veloso.

TGA Q500 TA Instruments, was used to perform the thermogravimetric analysis (TGA) using a 10 ^{o}C/min heating rate under a nitrogen flow, which was changed to oxygen from 800 ^{o}C. DSC Q2000 TA was used to carry out differential scanning calorimetry (DSC). The sample was sealed in an aluminum pan, and measured at a scanning rate of 10 ^{o}C/min under a nitrogen flow. Temperatures were taken from the onset of the transition.

Preparation and measurement of devices:

Commercially available interdigital Au electrodes (15x15 mm^2) from Fraunhofer IPMS were used. High doped n-type silicon was employed as gate electrode. A 30 nm Au electrode with a 10 nm high work function adhesion layer (ITO) (structured by lift-off technique) was patterned as source and drain electrodes respectively on the gate dielectric of 230-nm thermal-oxidized SiO_2. First, the electrodes were cleaned one by one by ultrasonication with electronic grade acetone and isopropanol and dried under compressed N_2. Then, the electrodes were treated with oxygen plasma for 15 minutes. To form self-assembled monolayers (SAMs) of octadeciltrichlorosilane (OTs) on the SiO_2 surface, the substrates were dipped into a solution of OTs (4 mM) in toluene and heated at 50 ^{o}C during 30 minutes. The modified electrodes were subsequently washed with chloroform and dried for 1 hour at 80 ^{o}C. Finally, the substrates were cleaned again with electronic grade acetone and isopropanol and dried with N_2.

40-nm thick compound **1** films were deposited by vacuum thermal deposition in an ultra high vacuum (UHV) evaporator (base pressure <10^{-9} mbar)) while the substrate temperatures were controlled at 25 ^{o}C, 80^{o}C, and 120^{o}C respectively. The electrical characterization of the devices was performed using a Keithley 4200 semiconductor analyser system connected to Lakeshore probe-station in vacuum at room temperature

without light. The samples were exposed to air before being introduced in the vacuum probe station for a time smaller than 30 minutes.

The mobility of each electrode was calculated in the saturation regime using Equation S1: [1]

$$I_{DS,sat} = \frac{C_i W}{2L} \mu_{FE} (V_{GS} - V_T)^2 \qquad \textbf{(Equation S1)}$$

Where μ_{FE} is the field-effect mobility, C_i is the capacitance per unit area of the dielectric layer, L is the channel length, W is the channel width, V_T is the threshold voltage and V_{GS} is the gate-source bias.

Atomic Force Microscopy (AFM):

Images in Figure X were taken by a commercial Agilent Atomic Force Microscope (AFM) with commercial Bruker NCHV tips in tapping mode. The scanned area of the samples was 5μm × 5μm with 512 points/lines resolution.

2. Synthesis and characterization of compounds 1 and 5:

Compound 5:

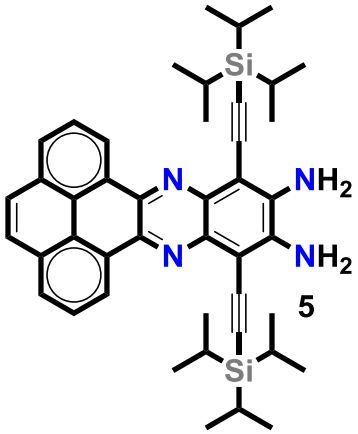

5

To a solution of compound **2** (252 mg, 0.348 mmol) in dry THF (10 mL), $LiAlH_4$ (44 mg, 1.16 mmol) was added at 0 ^oC under nitrogen atmosphere. Once completed the addition, the ice bath was removed and the mixture was stirred at room temperature overnight. The reaction was quenched by adding a saturated NH_4Cl solution and the aqueous layer was extracted with CH_2Cl_2. The organic layer was washed with water, dried over Na_2SO_4 and evaporated. The crude product was dissolved in CH_2Cl_2 and precipitated with hexanes to obtain diamine **2** as a dark yellow solid (228 mmol, 0.327 mmol, 94%). ^{1}H-NMR (400 MHz, $CDCl_3$) δ (ppm): 9.67 (d, J = 7.6 Hz, 2H), 8.24 (d, J = 7.5 Hz, 2H), 8.07-7.99 (m, 4H), 4.82 (s, 4H), 1.40-1.26 (m, 42 H). ^{13}C-NMR (100 MHz, $CDCl_3$) δ (ppm): 142.7, 140.4, 139.5, 131.3, 130.1, 127.9, 127.1, 126.4, 125.7, 123.5, 103.9, 103.7, 101.0, 19.0, 11.5. MS (MALDI-TOF) m/z: calc. for $C_{44}H_{54}N_4Si_2$ $[M^{+\cdot}]$: 694.39; found: 694.30. Calc. for $C_{44}H_{54}N_4NaSi_2$ $[M+Na]^+$: 717.38; found: 717.29.

Compound 1:

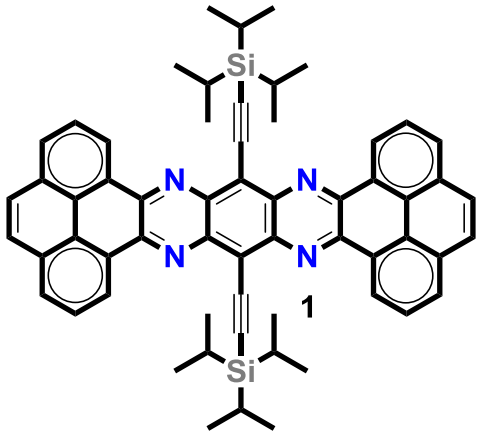

To a flask with a mixture of diamine **5** (51.6 mg, 0.074 mmol) and pyrene diketone 3(17.3 mg, 0.074 mmol), acetic acid (5 mL) was added, and the mixture was heated to 80 ^{o}C. After stirring for 72 hours, reaction was stopped and the resulting solid was filtered off, washing with dichloromethane. The purple precipitate was recrystallized in o-DCB and filtered off washing with o-DCB. Compound **3** was obtained as a bright reddish solid after drying for 72 h under vacuum (41 mg, 0.046 mmol, 62%). ^{1}H-NMR (500 MHz, $C_6D_4Cl_2$, temp) δ (ppm): 9.13 (d, J = 7.6 Hz, 4H), 7.40 (d, J = 7.6 Hz, 2H), 7.26 (dd, J_1 = 7.6 Hz, J_2 = 7.6 Hz, 4H), 7.12 (s, 4H), 0.86-0.77 (m, 36 H), 0.44-0.38 (m, 6 H). MS (MALDI-TOF) m/z: calculated for $C_{60}H_{59}N_4Si_2$ $[M+H]^+$: 891.43; found: 891.70.

3. NMR spectra for compounds 1 and 5:

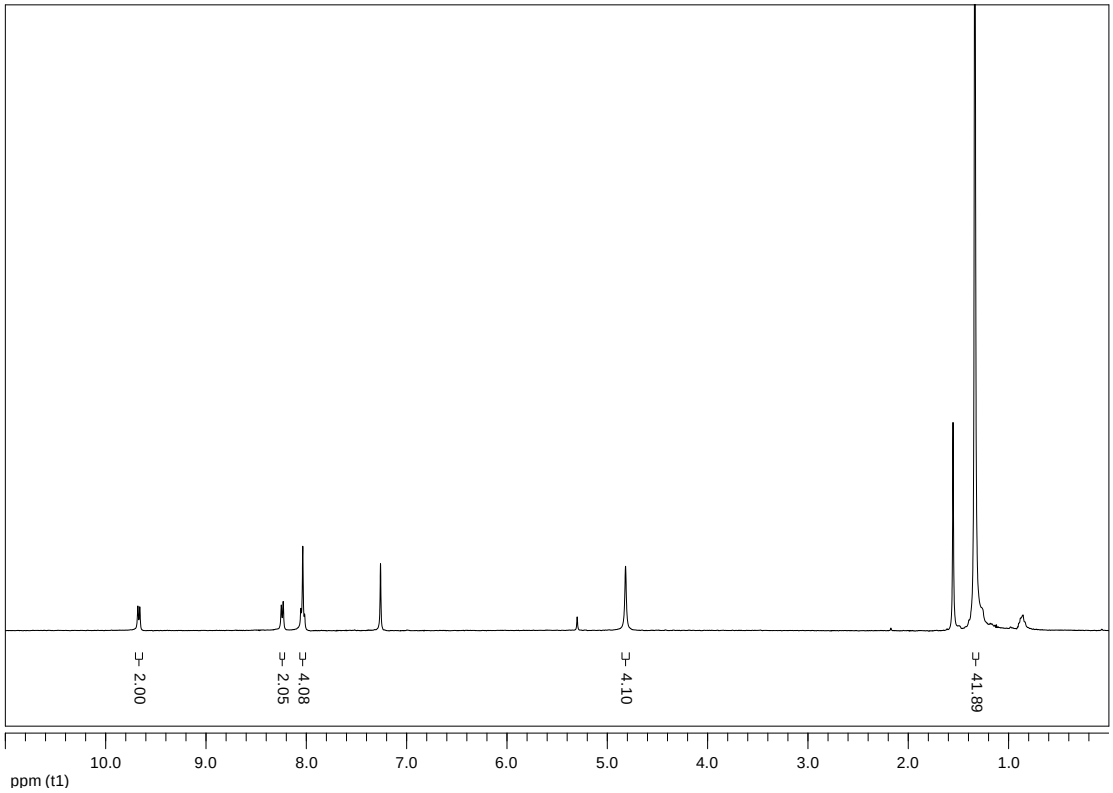

Figure S1. ^{1}H-NMR spectrum of compound **5** (400 MHz, $CDCl_3$).

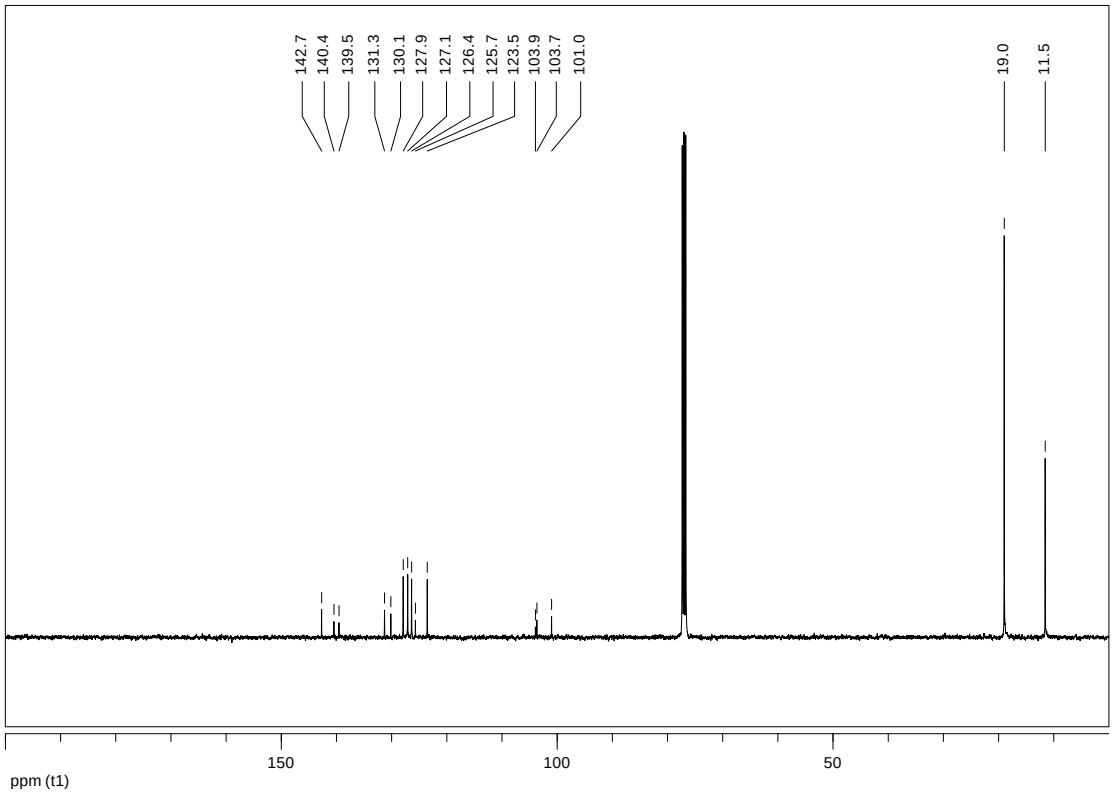

Figure S2. ^{13}C-NMR spectrum of compound **5** (100 MHz, $CDCl_3$).

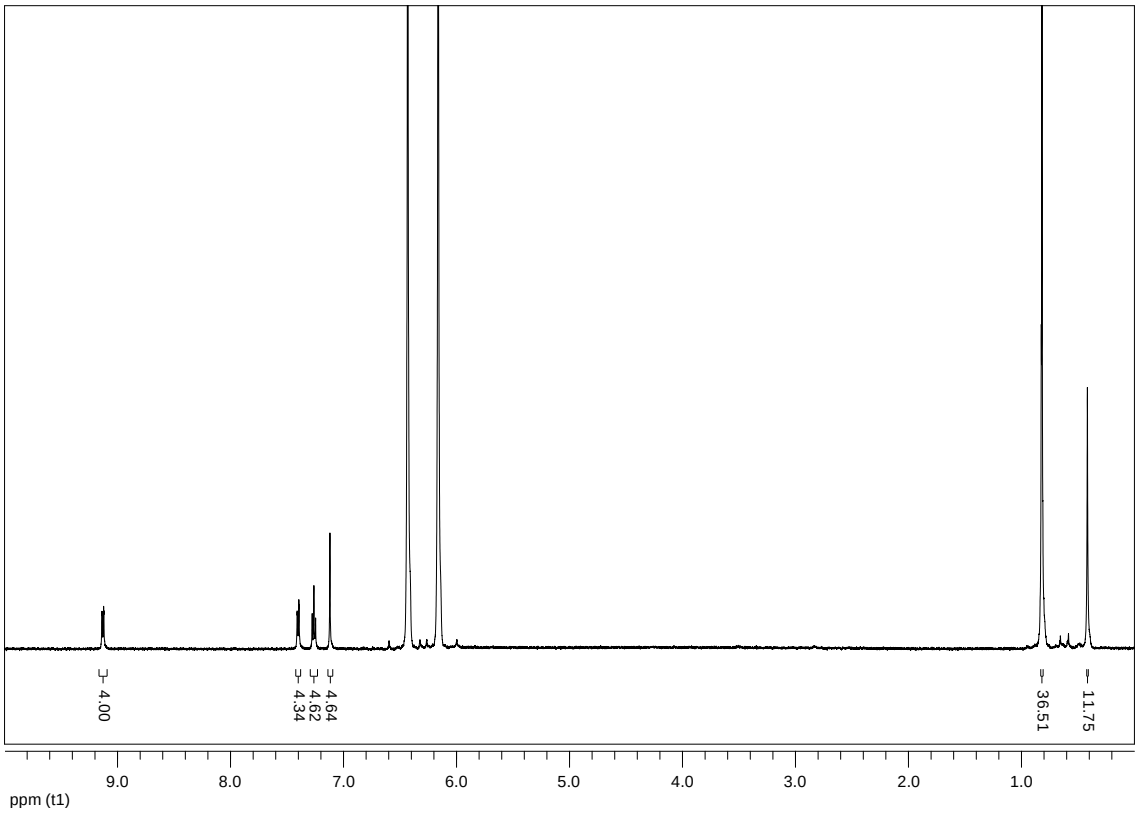

Figure S3. ^{1}H-NMR spectrum of compound **1** (500 MHz, $C_6D_4Cl_2$).

4. Thermal behavior of compound 1:

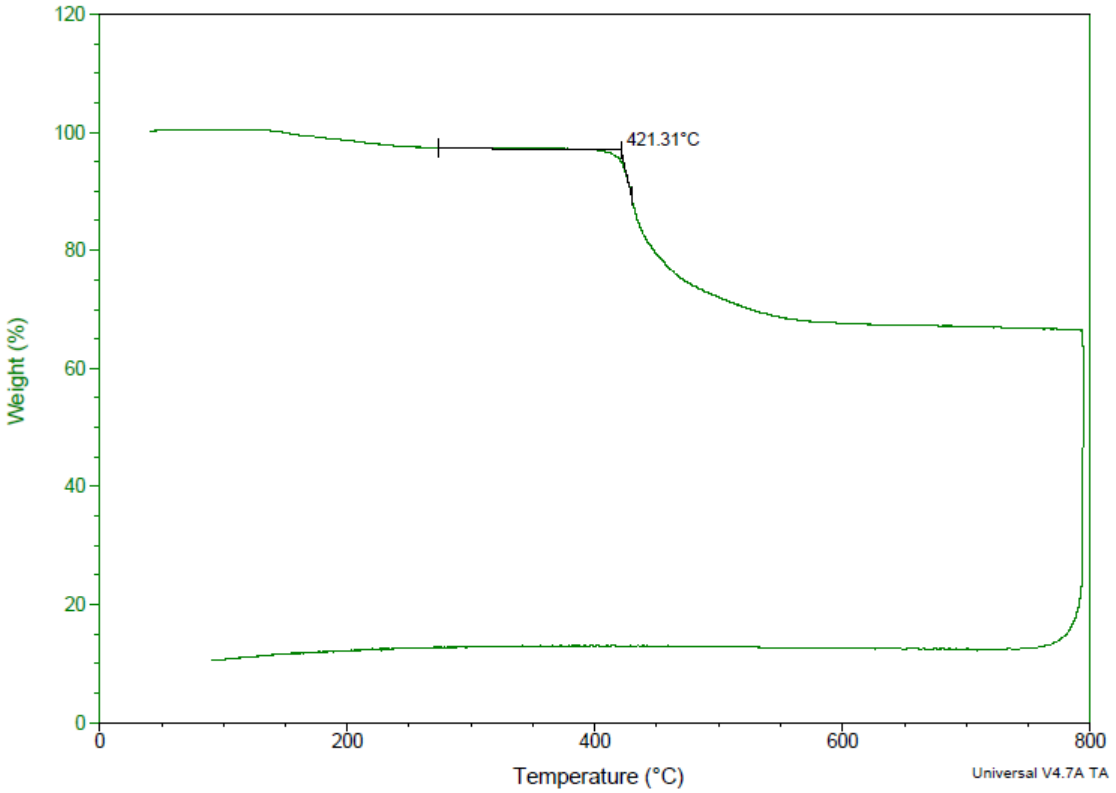

Figure S7. Thermogravimetric analisys (TGA) of compound **1** (10^{o}C/min, N_2 flow).

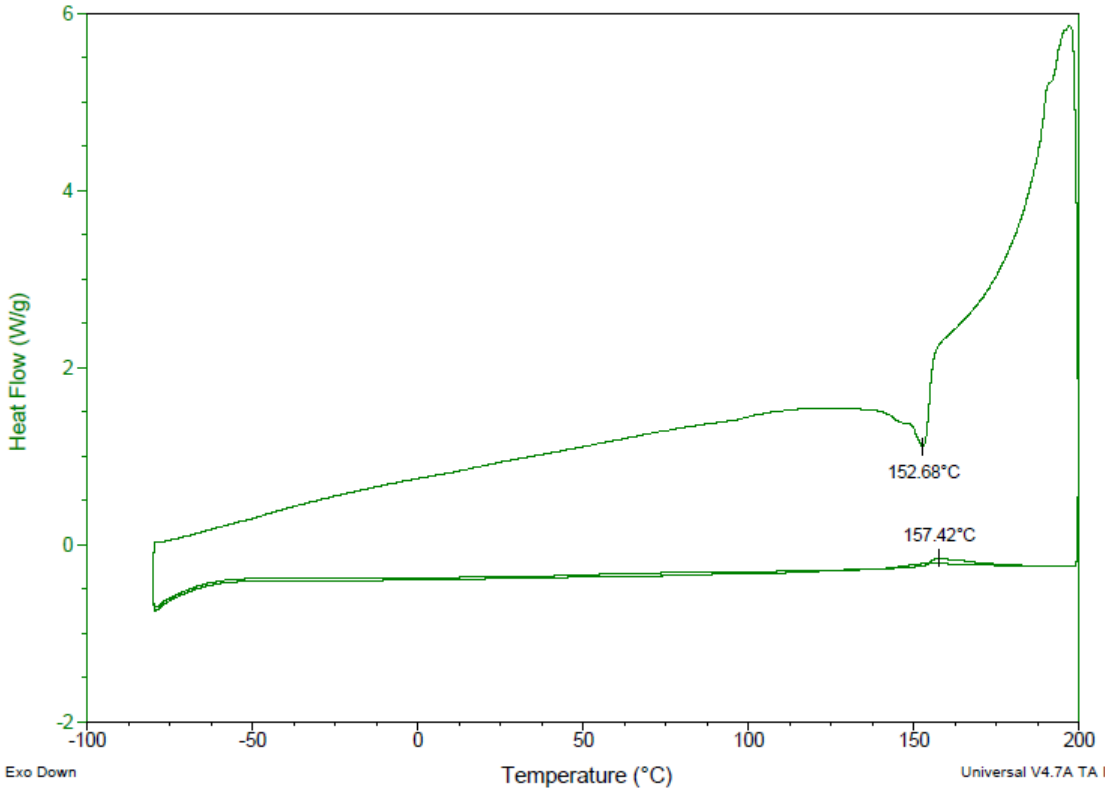

Figure S8. Differential Scanning Calorimetry of compound **1** (10^{o}C/min, N_2 flow).

5. Devices:

Table S1. Parameters obtained from the measurement of the Organic Thin Film Transistors (OTFTs) of different channel width (W) and length (L), prepared using Compound **1** at different substrate temperatures (r.t, 80°C and 120°C). Values for Mobility, Threshold voltage (V_t) and on/off ratio current ($I_{on/off}$) for the different devices, as well as the average electron mobility for compound **1** at each substrate temperature (highlighted in red) are presented.

		Room temperature			80 °C			120 °C		
W (μm)	**L** (μm)	**Mobility** (cm^2/Vs)	V_t (V)	$I_{on/off}$ (A)	**Mobility** (cm^2/Vs)	V_t (V)	$I_{on/off}$ (A)	**Mobility** (cm^2/Vs)	V_t (V)	$I_{on/off}$ (A)
10000	2.5	$2.27\cdot10^{-7}$	-17	$5.2\cdot10^{2}$	$2.18\cdot10^{-7}$	-7	$9.8\cdot10^{2}$	$8.07\cdot10^{-9}$	-9	$0.5\cdot10^{2}$
		$2.69\cdot10^{-7}$	-11	$5.1\cdot10^{2}$	$2.30\cdot10^{-7}$	-7	$1.2\cdot10^{3}$	$1.10\cdot10^{-8}$	-10	$0.4\cdot10^{2}$
		$2.48\cdot10^{-7}$	-21	$5.7\cdot10^{2}$	$2.15\cdot10^{-7}$	-7	$1.6\cdot10^{2}$	$1.23\cdot10^{-8}$	-8	$0.6\cdot10^{2}$
		$2.38\cdot10^{-7}$	-10	$4.3\cdot10^{2}$	$4.80\cdot10^{-8}$	-----	-----	------	-----	------
10000	5	$1.02\cdot10^{-7}$	-16	$2.2\cdot10^{2}$	$9.76\cdot10^{-8}$	-11	$3.1\cdot10^{2}$	$5.41\cdot10^{-9}$	-18	$0.1\cdot10^{2}$
		$1.02\cdot10^{-7}$	-16	$0,7\cdot10^{2}$	$9.60\cdot10^{-8}$	-19	$1.8\cdot10^{2}$	$7.79\cdot10^{-9}$	-6	$0.2\cdot10^{2}$
		$9.60\cdot10^{-8}$	-16	$1,7\cdot10^{2}$	$9.60\cdot10^{-8}$	-10	$2.0\cdot10^{2}$	$7.17\cdot10^{-9}$	-4	$0.2\cdot10^{2}$
		$1.14\cdot10^{-7}$	-17	$0.8\cdot10^{2}$	$1.06\cdot10^{-7}$	-25	$1.5\cdot10^{2}$	$6.28\cdot10^{-9}$	-16	$0.3\cdot10^{2}$
10000	10	$6.16\cdot10^{-8}$	-26	$0.3\cdot10^{2}$	$7.56\cdot10^{-8}$	-17	$0.8\cdot10^{2}$	------	-----	------
		$5.81\cdot10^{-8}$	-26	$0.2\cdot10^{2}$	$7.80\cdot10^{-8}$	-31	$1.1\cdot10^{2}$	------	-----	------
		$4.96\cdot10^{-8}$	-27	$0.2\cdot10^{2}$	$7.80\cdot10^{-8}$	-29	$0.5\cdot10^{2}$	------	-----	------
		------	-----	-----	------	-----	------	------	-----	------
10000	20	-----	-----	------	$6.14\cdot10^{-8}$	-31	$0.3\cdot10^{2}$	------	-----	------
		-----	-----	------	$5.76\cdot10^{-8}$	-30	$0.3\cdot10^{2}$	------	-----	------
		-----	-----	------	$1.13\cdot10^{-7}$	-31	$0.2\cdot10^{2}$	------	-----	------
		-----	-----	------	$5.62\cdot10^{-8}$	-----	------	------	-----	------
		$1.42\cdot10^{-7}$			**$1.08\cdot10^{-7}$**			**$8.29\cdot10^{-9}$**		

6. DFT calculations

Frontier orbitals and energies

Geometries were minimized at the B3LYP level with the 6-31g(d,p) basis set. All minima were checked by frequency calculations. Frontier orbital energies were computed with the 6-311g+(2d,p) basis set with the B3LYP, PBE0 and BMK Hamiltonians. Calculations in vacuum and o-dichlorobenzene (ODCB) were performed.

Table S1 presents the frontier orbital energies and the HOMO-LUMO gaps for B3LYP, PBE0 and BMK in the gas phase and ODBC. The LUMO derived from electrochemistry (–3.80 eV) is well reproduced by the vertical Electron Affinity (EA) (–3.64 eV) and the LUMO eigenvalue (–3.51eV) at the B3LYP level in ODBC. In addition, the HOMO-LUMO gap (2.26 eV) and the gap (2.03 eV) at the B3LYP level are similar to the experimentally estimated value (1.99 eV).

Table S1. Frontier orbitals, vertical Ionization Potentials (IP) and Electron Affinities (EA), gap (EA+IP) and Koopman's Theorem (KT) gap at the B3LYP, PBE0 and BMK 6-311g+(2d,p) levels from B3LYP-6-31g(d,p) geometries. **All values in eV.**

		EA	-IP	gap (IP+EA)	LUMO	HOMO	KT gap (LUMO-HOMO)
B3LYP	**ODBC**	−3.62	−5.65	2.03	−3.51	−5.77	2.26
B3LYP	**vacuum**	−2.53	−6.61	4.08	−3.47	−5.68	2.21
BMK	**ODBC**	−3.66	−5.92	2.26	−3.11	−6.49	3.38
BMK	**vacuum**	−2.50	−6.84	4.34	−3.01	−6.35	3.34
PBE0	**ODBC**	−3.72	−5.77	2.05	−3.5	−6.01	2.51
PBE0	**vacuum**	−2.57	−6.68	4.11	−3.4	−5.87	2.47

The Ionization Potential (IP) and the Electron Affinity (EA) values are quite similar for all three Hamiltonians. For B3LYP, the HOMO and LUMO energies in vacuum and ODBC show the best correlation with the corresponding IP and AE in ODBC, outranking PBE0 and BMK. In fact, for these systems, the HOMO and LUMO eigenvalues at the B3LYP level represent good estimates for the IP and EA.

The geometry of the frontier orbitals is shown in Figure S9. In both the HOMO and LUMO orbitals, electronic density is mainly located in the central rings of the tetraazaheptazacene with less electronic density in the pyrene moieties. In addition, the acetylene moieties support electronic density in the HOMO and the LUMO. The electronic density for HOMO–1 extends on the central rings and in the pyrene moieties.

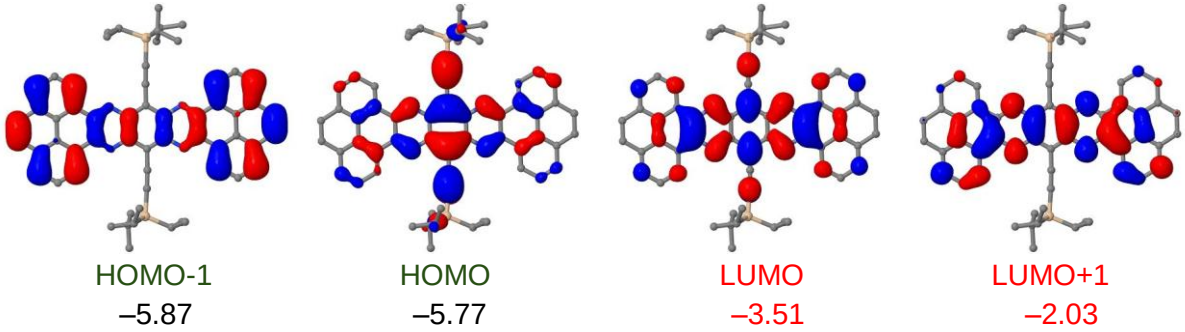

Figure S9. B3LYP-odbc-6311g+(2d,p)/B3LYP-odbc-6-31(d,p) level frontier orbitals and corresponding energies at the. **All values in eV.**

TD-DFT

The first 12 singlet excitations were computed with TD-DFT in ODCB and in vacuum, specifically at the B3LYP-odbc-6311g+(2d,p)/B3LYP-odbc-6-31(d,p) and the B3LYP-6311g+(2d,p)/B3LYP-6-31(d,p) levels (Table S2). The simulated spectra in vacuum and ODCB looked very similar and only the spectrum in ODCB will be discussed. The first two peaks and the most intense calculated transitions are due to the HOMO → LUMO and HOMO-1 → LUMO transitions at 662 and 632 nm respectively. Transitions from HOMO-2 and HOMO-3 show negligible intensities, which might be related to the fact that the largest electronic density is located in the pyrene moiety for these orbitals (Figure S10). The third excitation involves the HOMO-4 → LUMO and appears at 471 nm yet with a much lower intensity. Interestingly, the HOMO-3 and HOMO-4 orbitals are very similar to each other: they both share a similar and large electronic density

distribution in the pyrene moiety (Figure S10). However, the orbital phase in the two pyrene moieties on the HOMO-3 has opposite sign, and the HOMO-4 shows electronic density in the acetylene, in contrast to the HOMO-3. The higher wavelength transitions are due to excitations to the LUMO, since transitions to the LUMO+1 appear at wavelengths ≤400 nm due to the large energy gap between LUMO (–3.5 eV) and LUMO+1 (–2 eV) (Table S3).

Table S2. TD-B3LYP-odbc-6311g+(2d,p)/B3LYP-odbc-6-31(d,p) transitions.

Transition / nm	Transition / eV	Oscillator Strength	Major Contributions
662	1.87	0.155	HOMO→LUMO (99%)
632	1.96	0.7094	H-1→LUMO (99%)
471	2.63	0.0142	H-4→LUMO (99%)

Table S3. Frontier orbitals at the B3LYP-6-311g+(2d,p) level in ODCB and vacuum from B3LYP-6-31g(d,p) geometries. **All values in eV.**

	LUMO+2	LUMO+1	LUMO	HOMO	HOMO-1	HOMO-2	gap
ODCB	−2.03	−2.03	−3.51	−5.77	−5.87	−6.11	2.26
Vacuum	−2.00	−2.07	−3.47	−5.68	−5.94	−6.00	2.21

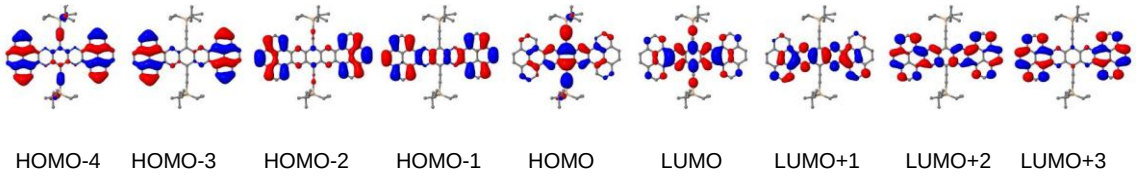

Figure S10. Frontier orbitals at the B3LYP-odbc-6311g+(2d,p)/B3LYP-odbc-6-31(d,p) level.

Comparison of experimental and TD-DFT excitation energies

The first two excitation energies at the TD-B3LYP level, 662 and 632 nm, are underestimated by up to 15% when compared with experimental values: 576 and 538 nm. Two other functionals were tried: PBE0 and BMK. The PBE0 Hamiltonian yields energies that are slightly closer to experiment, 633 and 602 nm, but still underestimates the excitation energies by up to 11% (Table S4). BMK shows the best performance with energies within 2% of experiment: 563 nm and 527 nm (Table S5 and Figure S11). The first two transitions with all Hamiltonians are from the HOMO and HOMO-1 to the LUMO and present the same intensity ratio: 22%. The variation of excitation energies follows the same trend observed in the HOMO-LUMO gap: B3LYP < PBE0 < BMK.

Table S4. TD-PBE0-odbc-6311g+(2d,p)/B3LYP-odbc-6-31(d,p) transitions.

Transition (nm)	Transition (eV)	Oscillator Strength	Major Contributions
633	1.96	0.1718	HOMO→LUMO (99%)
602	2.06	0.7823	H-1→LUMO (99%)
438	2.77	0.0159	H-4→LUMO (98%)

Table S5. TD-BMK-odbc-6311g+(2d,p)/B3LYP-odbc-6-31(d,p) transitions.

Transition (nm)	Transition (eV)	Oscillator Strength	Major Contributions
563	2.20	0.212	HOMO→LUMO (99%)
527	2.35	0.9787	H-1→LUMO (95%)
390	3.18	0.0204	H-4→LUMO (94%)

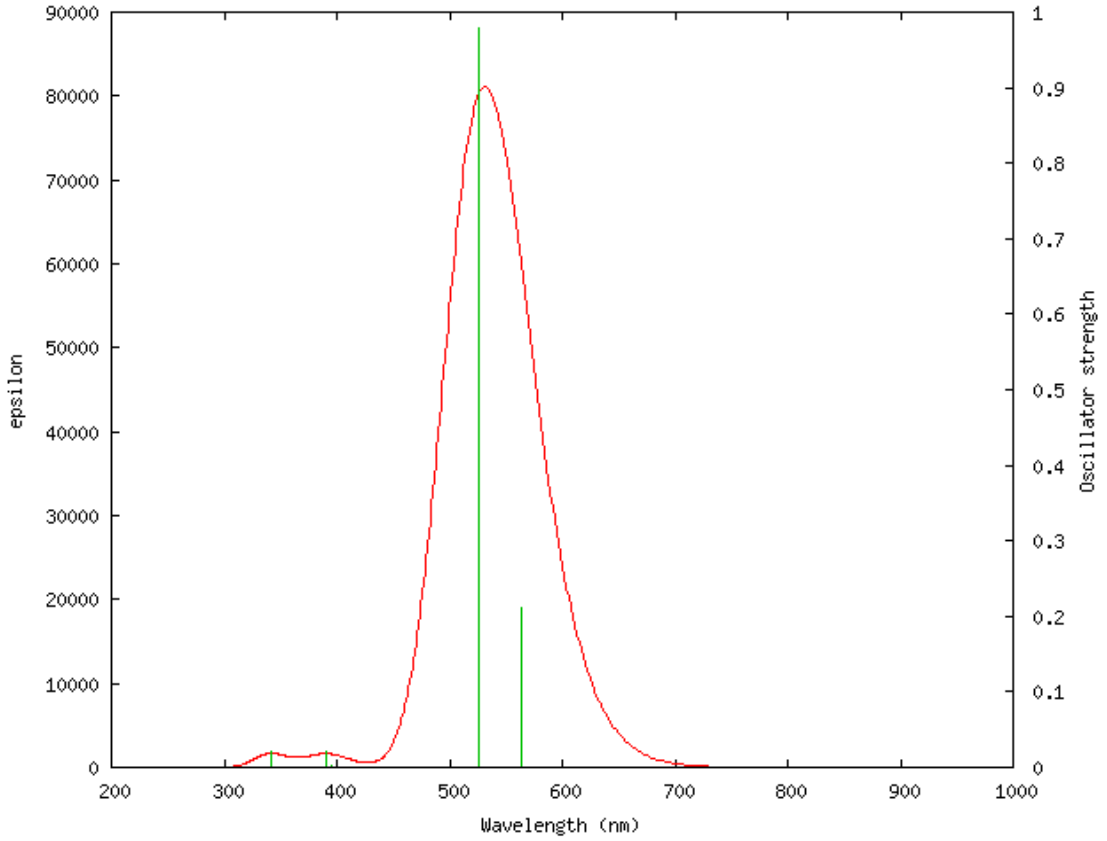

Figure S11. TD-BMK-odbc-6311g+(2d,p)/B3LYP-odbc-6-31(d,p) simulated spectrum.

References:

1. C. An, S. Zhou, M. Baumgarten *Cryst. Growth Des.*, 2015, **15**, 1934–1938.
2. J. Hu, D. Zhang, F. W. Harris *J. Org. Chem.*, 2005, **70**, 707–708.
3. A. B. Marco, D. Cortizo-Lacalle, C. Gozalvez, M. Olano, A. Atxabal, X. Sun, M. Melle-Franco, L. E. Hueso, A. Mateo-Alonso *Chem. Commun.*, 2015, **51**, 10754-10757.
4. F. M. Lee, A. Nathan, Y. Wu, B. S. Ong in *Organic Thin Film Transistor Integration: a Hybrid Approach* Wiley-VCH Verlag GmbH & Co. KGaA. 1st. edn., 2011, ch 2.